ARTICLE Open Access

# 0.32 mHz frequency mismatch of micro-shell resonator gyroscope without tuning electrodes achieved by ultra-precision mechanical trimming

Sheng Yu¹, Xianfeng Huang¹, Jiangkun Sun₀¹™, Peng Xie¹, Kun Lu¹, Yongmeng Zhang¹™, Xuezhong Wu¹ and Dingbang Xiao₀¹™

# **Abstract**

The frequency mismatch caused by material defects and geometric errors during the manufacturing process is a critical factor limiting the performance of micro-shell resonator gyroscope (MSRG). Compared with other MEMS gyroscopes, the frequency mismatch of MSRG can fundamentally be reduced by mechanical trimming. However, it is challenged by the precise characterization. Previous studies about the characterization of frequency mismatch are almost based on frequency spectrum analysis and sweeping, which can only meet the requirement of trimming efficiency of over 100 mHz, limited by the signal noise and temperature drift. In this paper, a novel characterization method of frequency mismatch based on the quadrature-control force under the self-precession mode is proposed to meet the requirement of high-precision mechanical trimming. Furthermore, the phase errors which affect the accuracy of characterization is analyzed, and methods for the correction of phase errors are proposed. Based on this characterization method, 0.32 mHz frequency mismatch of micro-shell resonator is achieved by mechanical trimming, which is the best-reported performance for mechanical trimming of MEMS gyroscopes so far. More importantly, this novel characterization method can be applied for other kinds of resonators which can be mechanical trimmed.

#### Introduction

The micro-shell resonator gyroscope (MSRG) is inspired by the hemispherical resonator gyroscope (HRG), with advantages of small size, low power consumption, and cost-effectiveness. It exhibits significant application potential in small guided weapons and unmanned systems<sup>1–3</sup>. The frequency mismatch, which is inevitably caused by material defects and manufacturing errors during the manufacturing process of micro-shell resonator, represents the difference of the resonant frequencies between two  $n = 2 \text{ modes}^{4,5}$ . It is a critical factor for the improvement of MSRG performance, which has negative effects on the mechanical sensitivity, and causes bias drift. Therefore, it is necessary to develop a high-precision frequency mismatch trimming methods for

mode match to improve the performance of the gyroscope.

Electrostatic and mechanical trimming methods are instrumental in reducing frequency mismatch for microshell resonators. Electrostatic trimming method leverages the electrostatic negative stiffness effect to regulate the local stiffness of the micro-shell resonator by applying a direct voltage on the tuning electrodes, achieving frequency mismatch trimming without physically modifying the resonator structure<sup>6,7</sup>. The frequency mismatch of MSRG can be reduced from 7 Hz to <0.1 Hz by applying a tuning voltage over 50 V on the tuning electrodes<sup>8</sup>. However, this method needs the incorporation of additional tuning electrodes, and the applied voltage may bring extra instable factors to the system especially under different temperatures<sup>9,10</sup>. Mechanical trimming can fundamentally reduce frequency mismatch by directly altering the mass or stiffness of micro-shell resonator, which can get rid of the tuning electrodes and enable all electrodes to be dedicated solely to detection and

Correspondence: Jiangkun Sun (sunjiangkun15@nudt.edu.cn) or Yongmeng Zhang (zhangym@nudt.edu.cn) or Dingbang Xiao (dingbangxiao@nudt.edu.cn)

<sup>1</sup>National University of Defense Technology, Changsha 410073, China

© The Author(s) 2025

Open Access This article is licensed under a Creative Commons Attribution-NonCommercial-NoDerivatives 4.0 International License, which permits any non-commercial use, sharing, distribution and reproduction in any medium or format, as long as you give appropriate credit to the original author(s) and the source, provide a link to the Creative Commons licence, and indicate if you modified the licensed material. You do not have permission under this licence to share adapted material derived from this article or parts of it. The images or other third party material in this article are included in the article's Creative Commons licence, unless indicated otherwise in a credit line to the material. If material is not included in the article's Creative Commons licence and your intended use is not permitted by statutory regulation or exceeds the permitted use, you will need to obtain permission directly from the copyright holder. To view a copy of this licence, visit http://creativecommons.org/licenses/by-nc-nd/4.0/.

actuation functions, enhancing the sensing SNR and driving efficiency. Precise frequency mismatch characterization followed by refined mass removal is essential for high-precision mechanical trimming. The characterization of frequency mismatch of MSRG are almost based on frequency spectrum analysis and sweeping, which can only meet the requirement of trimming efficiency of over 100 mHz<sup>11-13</sup>. Besides, the characterization methods based on frequency output under self-precession mode are widely used in MSRG, and a 5 mHz frequency mismatch trimming can be achieved<sup>14</sup>. Nevertheless, these methods have the limitations of high-level noise and frequency drift with temperature, which cannot meet the requirement of characterizing frequency mismatch below 1m Hz. Additionally, mechanical grinding process, chemical etching trimming process, micro ultrasonic machining process are also widely employed in frequency mismatch trimming of various resonator structures<sup>15–17</sup>. But these methods are constrained by the mathematical and physical limitations of the removal functions, hindering their ability to meet the stringent accuracy requirements of the below 1 mHz frequency mismatch trimming. To date, there have been no reported cases of achieving the frequency split of micro-shell resonator to below 1 mHz by mechanical trimming, whereas the hemispherical resonator has been demonstrated such precision. For coated hemispherical resonator, a frequency split and azimuth of stiffness axis identification model based on the vibration envelope and spectral analysis is widely employed, and frequency split can be reduced to 0.6 mHz combining with ion beam etching process<sup>18</sup>. The frequency mismatch of uncoated hemispherical resonator can be identified by the high precision orbital parameter identification algorithm based on nonlinear least square method has been proposed, and the frequency split of resonators can be reduced to 0.05 mHz based on the focus ion beam etching process<sup>19</sup>. However, these methods are not applicable to micro-shell resonator with small size and lower Q-factors.

In this paper, 0.32 mHz frequency mismatch of MSRG without tuning electrodes is achieved by ultra-precision mechanical trimming with femtosecond laser process. And the frequency mismatch of MSRG is characterized based on the quadrature-control force under the self-precession mode. The characterization model of frequency mismatch with the phase errors is established based on Lynch's theory, which subsequently facilitates the analysis of the effects of phase errors on characterization accuracy, leading to the proposal of identification and correction methods for phase errors. The aforementioned methods are verified by the simulations and experiments. Finally, experiments results demonstrate that 0.32 mHz frequency mismatch trimming of micro-shell resonator can be achieved by using an online femtosecond-laser mechanical-trimming platform

combining with the proposed characterization method. Furthermore, this method can also be widely applied to other kinds of resonator structures to reduce the frequency mismatch.

# Methods and analysis

## Description of structure and effects of frequency mismatch

The MSRG consists of micro-shell resonator and electrode substrate which are made of fused silica with a low coefficient of thermal expansion to ensure stable resonance properties, shown in Fig. 1a. The micro shell resonator is fabricated by high temperature micro-glassblowing process and ultrafast laser ablation<sup>20–24</sup>. Electrode substrate consists of the driving and sensing electrodes manufactured by the MEMS planar process, shown in Fig. 1b. The micro-shell resonator is bonded to the electrode substrate through the anchor, and the inner surface of the micro-shell is plated with a metal film to improve the conductivity<sup>25</sup>. There are 48 teeth-shape structures distributed along the micro-shell resonator's circumference, forming capacitors with the planar electrodes to drive and sense the vibration mode. The equivalent mass of the vibrating mode can be primarily altered by removing or adding mass from the teeth-shape structure, which can avoid the complexity of the trimming algorithm caused by the mass-stiffness coupling, facilitating the efficient and highprecision mechanical trimming. Two n = 2 wineglass modes of the micro-shell resonator are selected as working modes, which can achieve long decay times of over 90 s and high Q-factors of over 2.13 M, as shown in Fig. 1c.

Due to the inherent rotational symmetry of micro-shell resonator, the MSRG exhibits operational versatility to work in both force-balanced or whole-angle modes. However, geometric errors and material non-uniformity of micro-shell resonator will cause non-uniform mass and stiffness distributions during the manufacturing process, resulting in an inevitable initial frequency mismatch that detrimentally impacts gyroscope performance. In the force-balanced mode, the zero bias of the gyroscope caused by the frequency mismatch is mathematically represented<sup>26</sup> as

$$\dot{\theta}_b = \frac{F_Q \Delta \phi}{SF} = \Delta \omega \sin(2\theta_\omega) \Delta \phi \tag{1}$$

Where  $F_Q$  denotes quadrature-control force, SF is scale factor,  $\Delta\phi$  represents phase error,  $\Delta\omega$  and  $\theta_\omega$  are frequency split and the azimuth of the stiffness axis, respectively. Analogously, in the whole-angle mode, the zero bias expression takes the form<sup>27</sup> as

$$\dot{\theta}_b = \frac{f_{qc}\Delta\phi}{R_{SF}} = \Delta\omega \sin 2(\theta - \theta_\omega)\Delta\phi \tag{2}$$

Where  $f_{qc}$  is quadrature-control force,  $R_{SF}$  represents force-to-rotation scale factor,  $\theta$  is the pattern angle.

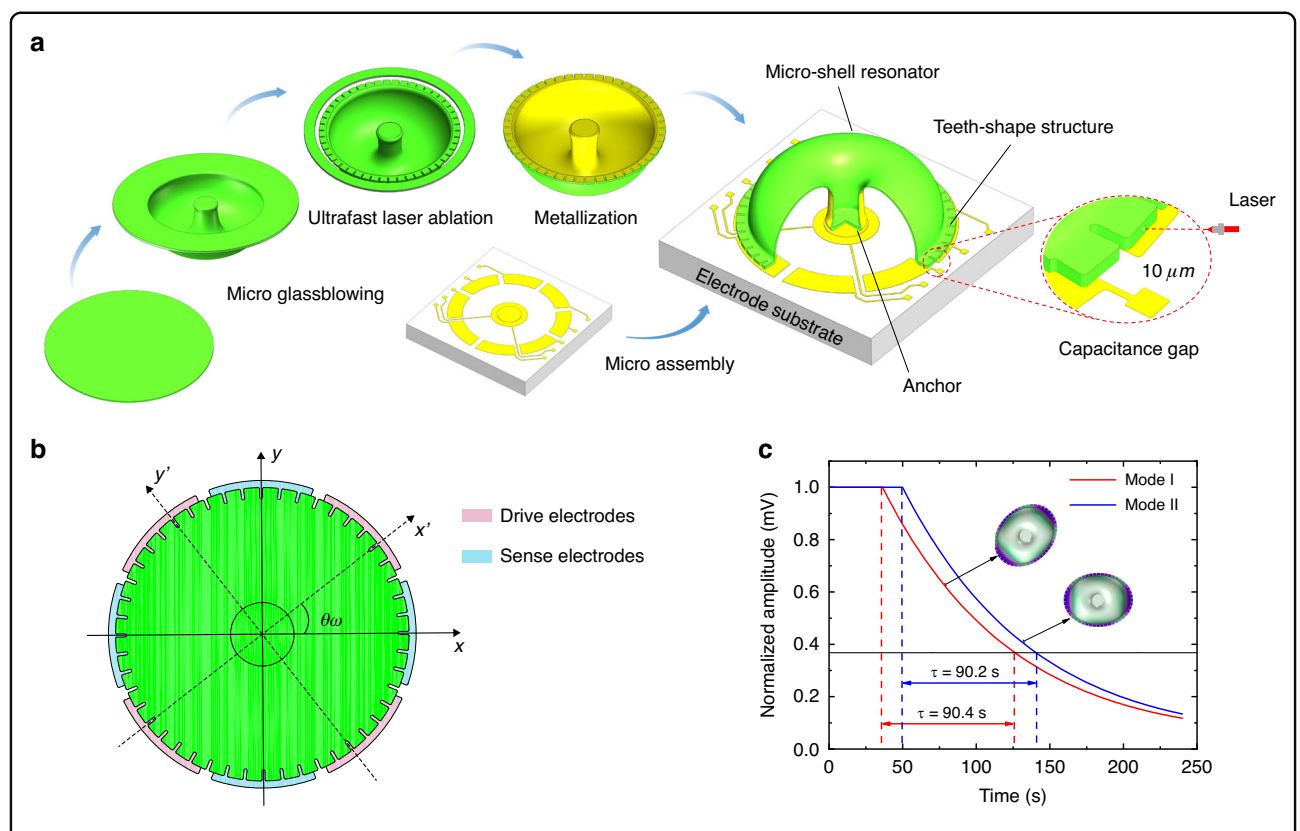


Fig. 1 The description of the micro-shell resonator. a Schematic illustration of the micro-shell resonator's fabrication process and structure of micro-shell resonator. b Electrode configuration of the MSRG without tuning electrode. c Ring-down tests of two n = 2 wineglass modes

Given a frequency split of 1 mHz and a reported optimal phase error of 10 ppm<sup>28</sup>, an estimation of the maximum zero bias can be derived as follows

$$\dot{\theta}_b = \Delta\omega\Delta\phi = 1 \times 10^{-3} \times 2\pi \times 57.3 \times 3600 \times (10 \times 10^{-6}) = 0.013^{\circ}/h$$
(3)

According to the analysis encapsulated in Eq. (3), achieving the accuracy standards demanded by navigation-grade gyroscopes (with a zero bias  $<0.01^\circ/h$ ) necessitates a reduction in the frequency mismatch below 1 mHz.

# Effects of trimming parameters on frequency mismatch

Based on the model of the mass and stiffness variations in the resonant structure, the mass variation of the microshell resonator is comprehensively analyzed, and a theoretical framework is established<sup>29</sup>. In practical resonators, there are mismatches in mass and stiffness, resulting in an initial frequency split known as  $\Delta\omega_0$  and the azimuth of high-frequency axis denoted as  $\psi_{01}$ , shown in Fig. 2a. To mitigate frequency mismatch, the mechanical trimming method is employed, which involves removing mass. When a mass trimming term  $\lambda_m \sum_m m_j e^{i4\phi_j}$  adding to the expression of the initial frequency mismatch, the

frequency mismatch after trimming can be mathematically represented as

$$\Delta\omega_1 e^{i4\psi_1} = \Delta\omega_0 e^{i4\psi_{01}} + \lambda_m \sum_{j=1}^{N_m} m_j e^{i4\phi_j}$$
 (4)

Where  $\lambda_m=((1-\alpha_2^2)\omega_0)/((1+\alpha_2^2)M_0)$  is a coefficient dependent on the resonator's mechanical properties and can be empirically determined through trimming experiments. Specifically, it can be determined by using femtosecond lasers to ablate varying masses along the azimuth of the stiffness axis. Subsequently, the corresponding reduction in frequency split is measured for each amount of mass removed. Finally, the resultant data is fitted with a linear function to establish the calibration.  $\alpha_2$  represents the ratio of the radial amplitude to the tangential amplitude of the resonant structure,  $\omega_0$  and  $M_0$  denote the resonant frequency and mass.  $m_j$  and  $\phi_j$  represent trimming mass and azimuth.

To evaluate the impact of trimming parameters, the numerical simulations are conducted in accordance with the theoretical model. For the simulations, the initial frequency split  $\Delta\omega_0$  is set to 100 mHz and the azimuth of low-frequency axis is assumed to be 45°, and  $\lambda_m$  is calibrated to be 0.2 mHz/ng based on experimental data.

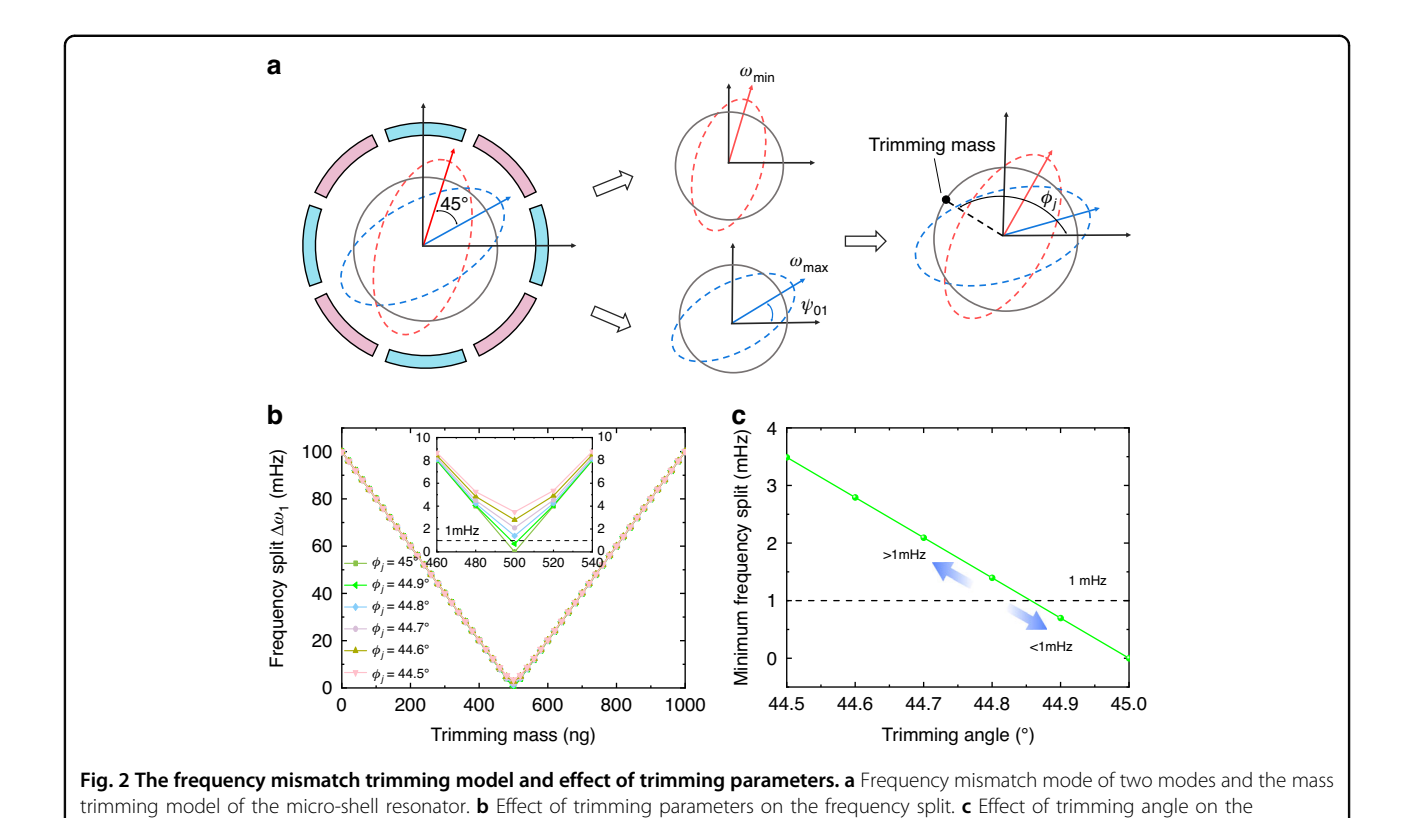


Figure 2b shows the variations in frequency mismatch as a function of trimming parameters. Notably, a precise mass removal of  $500 \pm 5 \, \mathrm{ng}$  at the azimuth of low-frequency axis is necessary to reduce the frequency split to <1 mHz, highlighting the necessity for nanogram-level accuracy in mass removal, by femtosecond lasers. And it is essential to realize a characterization error of stiffness axis azimuth of <0.2° to achieve frequency split trimming below 1 mHz, as shown in Fig. 2c. This precision requirement underscores the importance of employing a highly precise characterization method of frequency mismatch.

## Characterization method of frequency mismatch

frequency split

The core idea of this novel characterization method for frequency mismatch of micro-shell resonator is based on the self-precession mode, which is an operation mode of the whole-angle gyroscopes. The control system of whole-angle MSRG comprises a micro-shell resonator and an electronic control circuitry, as depicted in Fig. 3. Specifically, the micro-shell resonator serves as a Coriolis force-sensitive element which can sense rotational motion. Regarding the electronic control system, it is constructed by utilizing the printed circuit boards (PCB) and a field-programmable gate array (FPGA) platform. The PCB incorporates both digital-to-analog converters (DAC) and analog-to-digital converters (ADC), facilitating the

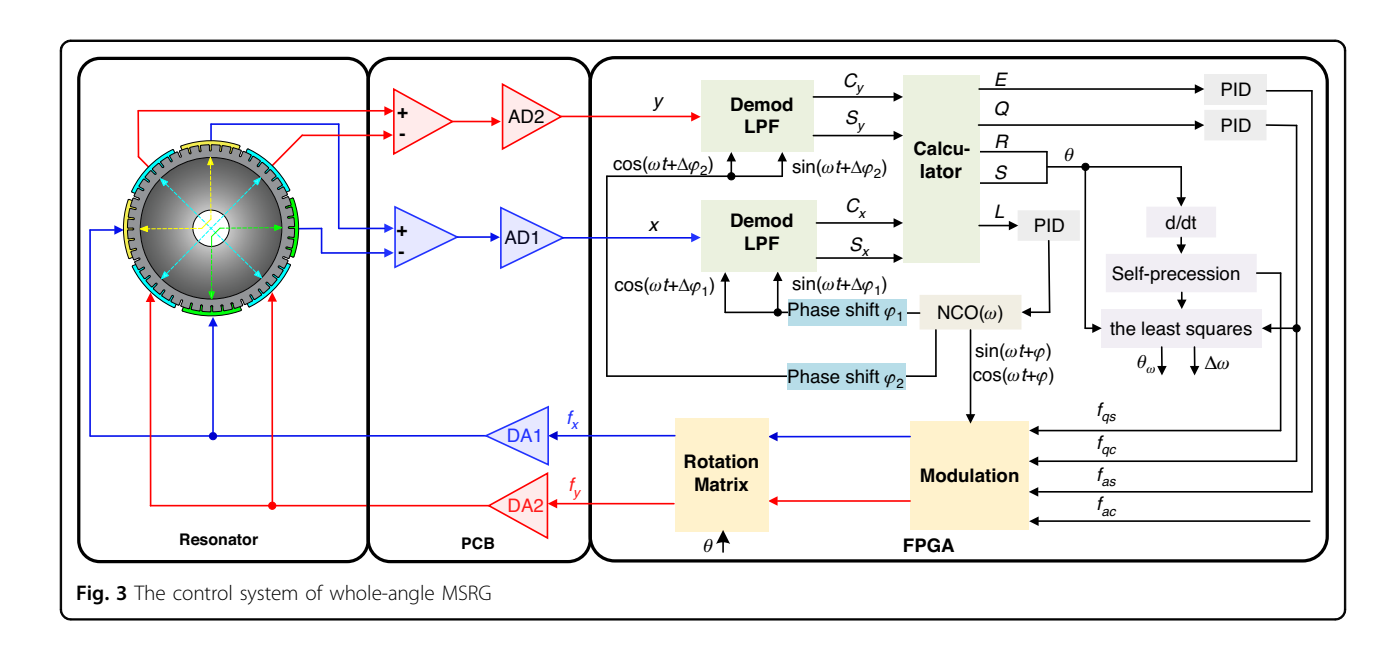
detection and actuation of the resonator vibrations. The FPGA platform is tailored to perform various digital signal processing and execute intricate control algorithms, ensuring robust system performance.

According to Lynch's theory<sup>30</sup>, under the whole-angle mode, the relationship between the control forces and control variables of vibration can be formulated as follows

$$\begin{split} \dot{E} &= -[\frac{2}{7} + \Delta(\frac{1}{7})\cos 2(\theta - \theta_{\tau})]E - \frac{\sqrt{E}}{\omega}f_{as} \\ \dot{Q} &= -\frac{2}{7}Q - \Delta\omega\sin 2(\theta - \theta_{\tau})E + \frac{\sqrt{E}}{\omega}f_{qc} \\ \dot{\theta} &= -k\Omega + \frac{1}{2}\Delta(\frac{1}{7})\sin 2(\theta - \theta_{\tau}) + \frac{1}{2}\Delta\omega\cos 2(\theta * - \theta_{\omega})\frac{Q}{E} - \frac{f_{as}}{2\omega\sqrt{E}} \\ \delta\dot{\phi} &= \dot{\phi} + \frac{1}{2}\Delta\omega\cos 2(\theta - \theta_{\omega}) + \frac{1}{2}\Delta(\frac{1}{7})\sin 2(\theta - \theta_{\omega})\frac{Q}{E} + \frac{f_{ac}}{2\omega\sqrt{E}} \end{split}$$

$$(5)$$

Where E represents the energy, maintained by the energy-control loop, Q stands for quadrature error, suppressed to zero by the quadrature-control loop. And  $\theta$  and  $\delta\phi$  are the pattern angle and the phase difference between actuation and detection signals, respectively.  $\Omega$  is the input rotation rate, k is the angular gain of input rotation rate  $\Omega$ .  $\theta_{\tau}$  and  $\theta_{\omega}$  are the azimuths of the damping and stiffness principal axes respectively,  $\Delta\omega$  and  $\Delta(1/\tau)$  indicate the frequency split and damping mismatch of MSRG. The control forces  $f_{as}$ ,  $f_{qc}$ ,  $f_{qs}$  and  $f_{qc}$  represent the output forces of control loops of energy, quadrature, pattern angle and frequency, respectively.



As observed from Eq. (5), when a constant value of virtual rotating force  $f_{qs}$  is applied to the MSRG to induce a stable vibration mode precession rate  $\Omega_{\nu}$  in the absence of an external angular rate input, the quadrature-control force  $f_{qc}$  can be expressed as

$$f_{qc} = R_{SF} \times \frac{1}{2} \Delta \omega \sin 2(\theta - \theta_{\omega})$$
 (6)

where  $R_{SF}=-f_{qs}/\Omega_v=2\omega E^{1/2}$  represents force-to-rotation scale factor. The components  $\lambda_a$  and  $\lambda_b$  of  $f_{qc}$  versus  $sin2\theta$  and  $cos2\theta$  can be identified by the least squares method, and then the frequency split  $\Delta\omega$  and azimuth of stiffness axis  $\theta_\omega$  can be calculated as

$$\Delta\omega = \frac{2\sqrt{\lambda_a^2 + \lambda_b^2}}{R_{SF}}, \theta_\omega = \frac{1}{2}\arctan\left(\frac{\lambda_b}{\lambda_a}\right)$$
 (7)

Compared with the characterization method based on the frequency output under the self-precession mode, this method not only avoids the effect of temperature drift, but also has better SNR and resolution. However, this method cannot directly obtain the frequency mismatch, which may cause characterization errors. Therefore, it is necessary to analyze the sources of characterization errors and make corresponding corrections to achieve high-precision characterization.

# Analysis of the effects of phase error on characterization accuracy of frequency mismatch

The primary error source for the characterization method is phase error, which mainly comes from the phase delay of the analog circuitry and digital low-pass filters (LPF). In control electronics, a high-frequency carrier is employed to mitigate the effects of electrical interference and low-frequency coupling. In general, the sections of phase delay mainly include carrier demodulation, a capacitance-to-voltage converter, LPF, ADC, and DAC. When the phase error of x and y channels are  $\Delta\phi_1$  and  $\Delta\phi_2$  respectively, the quadrature-control force  $f_{qc}$  can be expressed as

$$f_{qc} = R_{SF} \times \frac{1}{2} \Delta \omega \sin 2(\theta - \theta_{\omega}) + f_{qs}$$

$$\times \left[ \frac{\sin \Delta \varphi_{1} + \sin \Delta \varphi_{2}}{2} + \frac{\sin \Delta \varphi_{1} - \sin \Delta \varphi_{2}}{2} \cos 2\theta \right]$$
(8)

Therefore, the calculated frequency split and azimuth of stiffness axis are respectively given by the following equations

$$\begin{split} \Delta\omega^{'} &= \frac{\sqrt{(R_{SF} \times \Delta\omega\cos2\theta_{\omega})^{2} + (f_{gp} \times \delta\Delta\phi - R_{SF} \times \Delta\omega\sin2\theta_{\omega})^{2}}}{R_{SF}} \\ &= \sqrt{(\Delta\omega)^{2} + (\Omega_{v} \times \delta\Delta\phi)^{2} - 2\Omega_{v}\delta\Delta\phi \times \Delta\omega\sin2\theta_{\omega}} \end{split} \tag{9}$$

$$\theta_{\omega}^{'} = \frac{1}{2} \arctan[\tan 2\theta_{\omega} - \frac{\Omega_{v} \delta \Delta \phi}{\Delta \omega \cos 2\theta_{\omega}}]$$
 (10)

where  $\delta\Delta\phi=\sin\Delta\varphi_1-\sin\Delta\varphi_2\approx\Delta\varphi_1-\Delta\varphi_2$  represents the difference of phase error between x and y channels.

On the basis of the above theoretical analysis, it is observed from Eqs. (9) and (10) that the characterization error of frequency split and azimuth of stiffness axis arise owing to the phase errors. The characterization error of frequency split caused by different phase errors under different  $\theta_{\omega}$  from 0° to 180° are

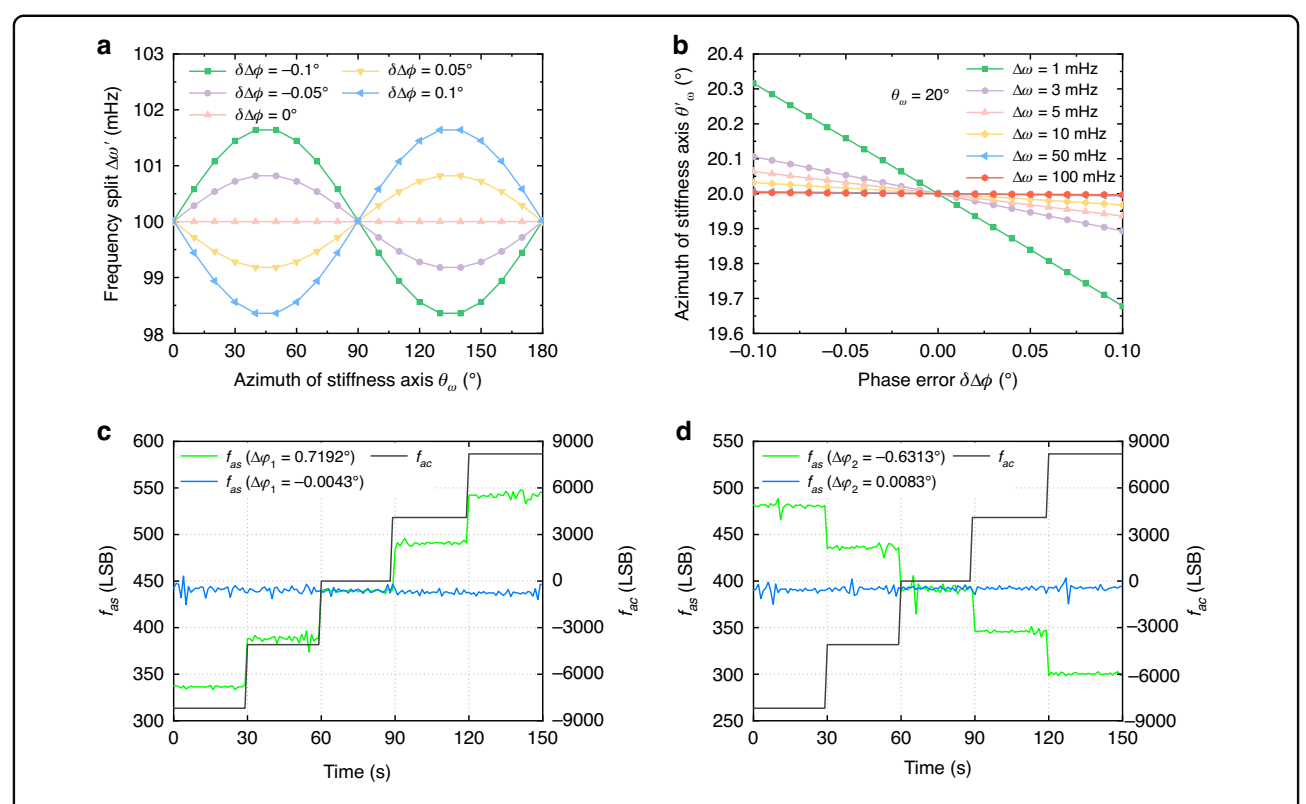


Fig. 4 The effects of phase error on characterization accuracy and the correction of the phase error. a Simulation results of frequency split characterization error under different phase error  $\delta\Delta\phi$ . **b** Simulation results of azimuth of stiffness axis under different phase error  $\delta\Delta\phi$ . **c** The control force  $f_{as}$  before and after the correction of phase error  $\Delta\phi_1$ . **d** The control force  $f_{as}$  before and after the correction of phase error  $\Delta\phi_2$ .

researched by simulation. As shown in Fig. 4a, the phase error will cause largest characterization error of frequency split under the azimuth of stiffness axis of 45° and 135°. In order to ensure the characterization precision of frequency split of below 1 mHz, the phase error must be to corrected to below 0.05°. To investigate the effects of the phase errors, simulations are conducted to analyze the characterization error of azimuth of stiffness axis caused by phase errors. During the simulation, the phase error  $\delta\Delta\phi$  is altered from  $-0.1^{\circ}$  to  $0.1^{\circ}$  to investigate the effects of different phase error  $\delta\Delta\phi$  under different initial frequency split from 1 mHz to 100 mHz, with the initial azimuth of stiffness axis is 20°. As shown in Fig. 4b, it is found that the phases error  $\delta\Delta\phi$  must be to corrected to below 0.06° in order to ensure that the characterization accuracy of the azimuth of stiffness axis is <0.2°, thereby meeting the requirements of frequency split trimming below 1 mHz from the mechanical trimming model above.

The identification method of the phase error is based on the relationship between the control forces  $f_{as}$  and  $f_{ac}.$  To be specific, under the assumption that the phase errors of x and y channels are respectively denoted by  $\Delta\phi_1$  and  $\Delta\phi_2,$ 

the control force  $f_{as}$  of the energy-control loop can be expressed as

$$\begin{split} f_{as} &= R_{SF} \times \left[ \frac{1}{\tau} + \frac{1}{2} \Delta(\frac{1}{\tau}) \cos 2(\theta - \theta_{\tau}) \right] \\ &+ f_{ac} \times \left[ \frac{\sin \Delta \varphi_1 + \sin \Delta \varphi_2}{2} + \frac{\sin \Delta \varphi_1 - \sin \Delta \varphi_2}{2} \cos 2\theta \right] \end{split} \tag{11}$$

To further analyze this relationship, the partial derivative of fas with respect to fac is derived as

$$\frac{\partial f_{as}}{\partial f_{ac}} = \frac{\sin \Delta \varphi_1 + \sin \Delta \varphi_2}{2} + \frac{\sin \Delta \varphi_1 - \sin \Delta \varphi_2}{2} \cos 2\theta \tag{12}$$

Specifically, by setting the angular parameter  $\theta$  to 0°, the equation (12) undergoes a simplification, yielding

$$\frac{\partial f_{as}}{\partial f_{ac}} = \sin \Delta \varphi_1 \tag{13}$$

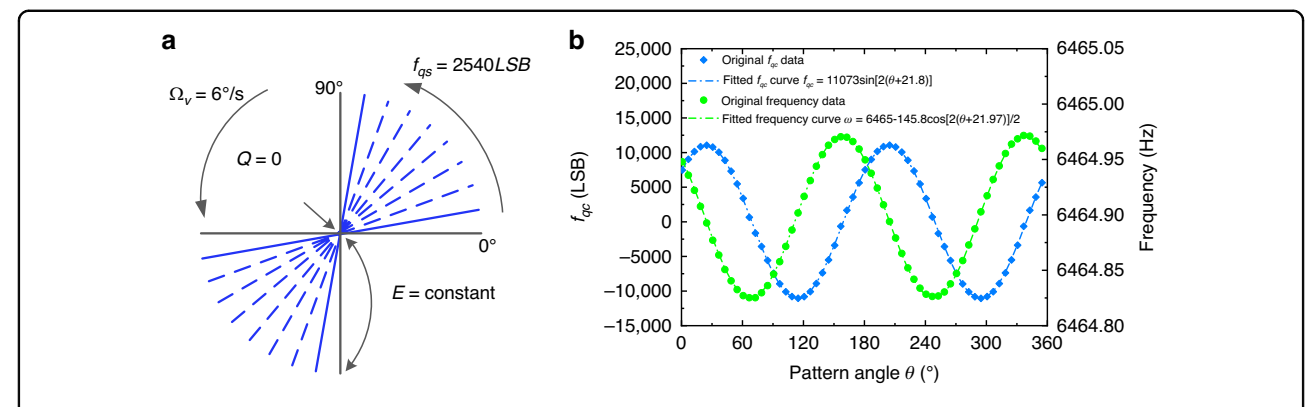


Fig. 5 The characterization of frequency mismatch based on the self-precession mode. a The self-precession mode. b Characterization results of frequency mismatch based on quadrature-control force and direct frequency output

Analogously, when  $\theta$  is set to 90°, the equation (12) is simplified as

$$\frac{\partial f_{as}}{\partial f_{ac}} = \sin \Delta \varphi_2 \tag{14}$$

From Eqs. (13) and (14), the phase errors of x and y channels are identified. And the phase errors are corrected by the phase shift module. Specifically, for x channel, the correction of phase error is carried out by shifting the NCO phase by  $\Delta \varphi_1$  and the output reference signal becomes  $cos(\omega t + \Delta \phi_1)$ instead of  $\cos(\omega t + \varphi)$ . The same principle is applied to y channel, as shown in Fig. 3. After the correction of phase errors, the frequency mismatch can be accurately characterized.

In order to verify this phase error identification and correction method, a micro-shell resonator gyroscope with an initial phase error of ~0.7° is chosen as the device for experiments. According to the Eq. (11), the amplitude of control force fas varies with the growth of control force fac, due to the phase error. During the experiments, the control force fas of the whole-angle gyroscope has been collected with a 1 Hz sampling rate for 30 s under every f<sub>ac</sub> value, ranging from -8196 LSB to 8196 LSB. The averaged value of fas is taken as the final output when the pattern angle  $\theta$  is controlled to stay at 0° or 90°, respectively. Subsequently, a linear function is employed to fit the results to obtain the phase errors. As shown in Fig. 4c, d, the original phase error  $\Delta \phi_1$  and  $\Delta \phi_2$  are found to be 0.7192° and  $-0.6313^{\circ}$ , respectively. When the phase errors are corrected by the phase shift module, the phase errors  $\Delta \phi_1$  and  $\Delta \phi_2$  respectively are reduced to  $-0.0043^{\circ}$  and 0.0083° satisfying the requirements of below 0.06° for high-precision characterization of frequency mismatch.

# **Experiments and results**

# Verification of the characterization of frequency mismatch

The characterization method of frequency mismatch based on the quadrature-control force under the self-precession mode is compared with the characterization method based on the direct frequency output to verify its effectiveness. According to the Eq. (5), when a constant rate of precession is applied to gyroscope and the quadrature quantity is suppressed to zero by the quadrature-control loop, the frequency output of the gyroscope at different pattern angle  $\theta$  can be presented as

$$\omega = \omega_0 - \frac{1}{2} \Delta \omega \cos 2(\theta - \theta_\omega) \tag{15}$$

The difference between the highest and lowest points of the curve is the frequency split  $\Delta\omega$ , and angles corresponding to the highest point and the lowest point are the stiffness axis azimuths. A micro-shell resonator gyroscope with a frequency split of >100 mHz is chosen as the device for experiments and the data is collected under stable temperature conditions in order to avoid the influence of temperature drift on the characterization from frequency output. As illustrated in Fig. 5, when a precession rate of 6°/s is applied to the gyroscope, the characterization result given by the direct frequency output is a frequency split of 145.80 mHz and the azimuth of stiffness axis of  $-21.97^{\circ}$ . Afterward, the frequency mismatch is obtained based on the quadrature-control force after the phase errors are corrected by the phase shift module with a frequency split of 145.31 mHz and the azimuth of stiffness axis of  $-21.80^{\circ}$ . The experimental results demonstrate that the frequency split given by the two characterization methods differs by 0.49 mHz, and the stiffness axis angle differs by <0.20°. Consequently, the method based on the quadrature-control force under the self-precession mode is effective and precise enough.

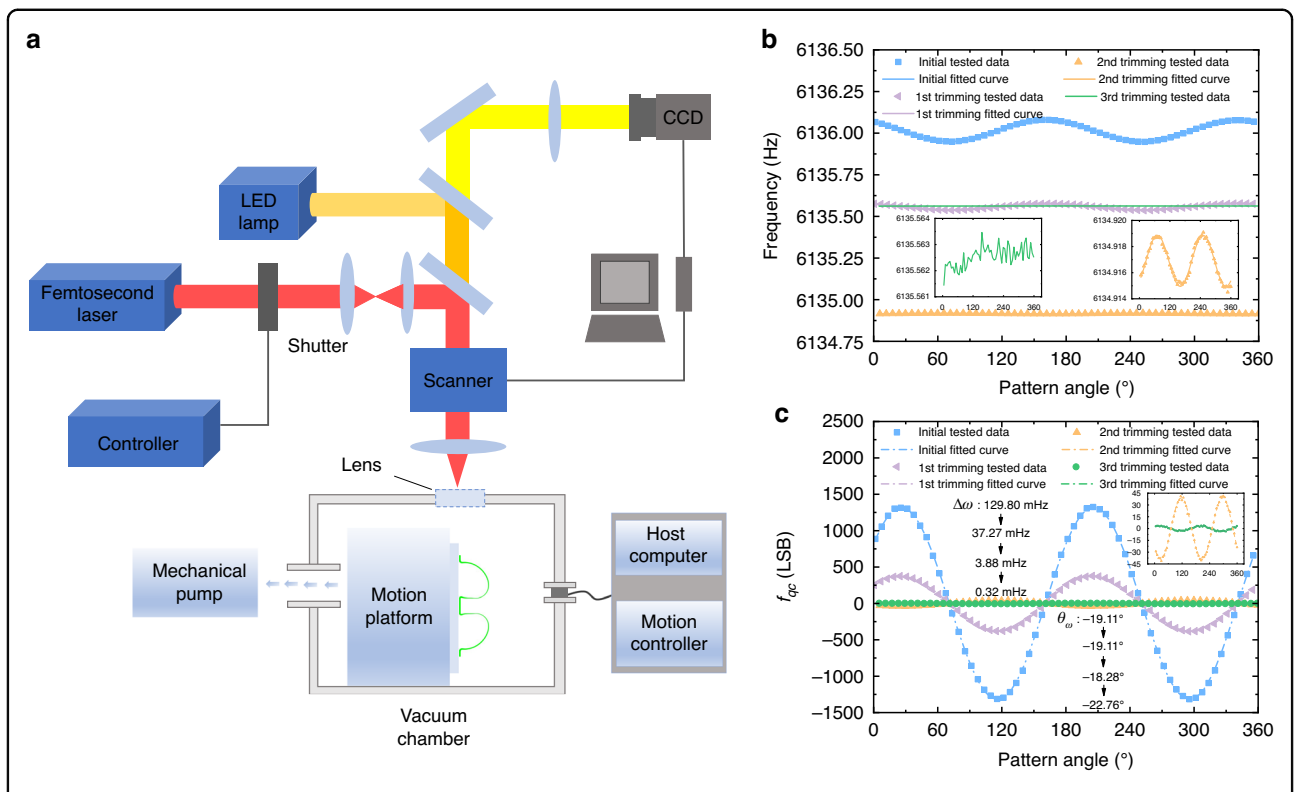


**Fig. 6 The illustration of trimming system and trimming results. a** Online femtosecond laser trimming system. **b** Test data of frequency during mechanical trimming of MSRG M01. **c** Test data of quadrature-control force  $f_{ac}$  during mechanical trimming of MSRG M01

# Femtosecond laser trimming system and frequency mismatch trimming process

In order to verify the proposed precise characterization and mechanical trimming method, an online trimming system based on femtosecond laser technology is built, as shown in Fig. 6a. The Pharos Ph1-20-0200-06-10 laser is employed for the precise mechanical trimming, featuring a wavelength of 343 nm, a laser power of 5 W, and a repetition rate of 100 kHz. In addition to the laser wavelength, other laser parameters are adjustable. The interaction of femtosecond laser with fused silica is very complicated. In order to avoid stress and metal film ablation caused by laser action during the trimming process, the method of controlled variables is used to optimize the laser parameters. The operation process of frequency mismatch trimming system has been described as follow: 1. a micro-shell resonator with control circuits is placed on a motion platform equipped with rotational and translational degrees of freedom, enabling the precise positioning of the low-frequency axis of the resonator directly beneath the femtosecond laser. 2. the frequency mismatch is characterized by the control system after correction for the phase errors. 3. the required mass at specific location of resonator is removed by the femtosecond laser according to the characterization results. After completing one turn trimming following the steps above, the frequency mismatch is measured again. If the results can not satisfy the requirement, the trimming procedures are repeated as described above. It should be noted that the scale factor will change due to the temperature effects. In order to avoid its influences on the characterization of the frequency split, the value of scale factor is identified and updated in real time by collecting the data of applied virtual rotating force fqs and responsive precession rate  $\Omega_{\rm v}$ . The entire system operates within a vacuum chamber with a vacuum degree of 0.1 Pa, which allows characterization and mass removal simultaneously to improve the mechanical trimming efficiency.

The MSRG M01with the resonant frequency of about 6135 Hz and initial frequency split of 129.80 mHz is chosen for trimming experiment, as depicted in Fig. 6b. It underwent three rounds of trimming, resulting in a reduction of the frequency split to below 1 mHz. Figure 6b, c depict the frequency and quadrature-control force variation during the trimming process. As shown in Fig. 6b, the resonant frequency changes from 6134 Hz to 6136 Hz due to the temperature drift, and the frequency mismatch cannot be directly characterized by frequency output when the frequency split is reduced to below 1 mHz. Simultaneously, the amplitude of quadrature-control force also gradually decreases, eventually reaching a state of minimal fluctuations, shown in Fig. 6c. After 3 rounds of trimming, the

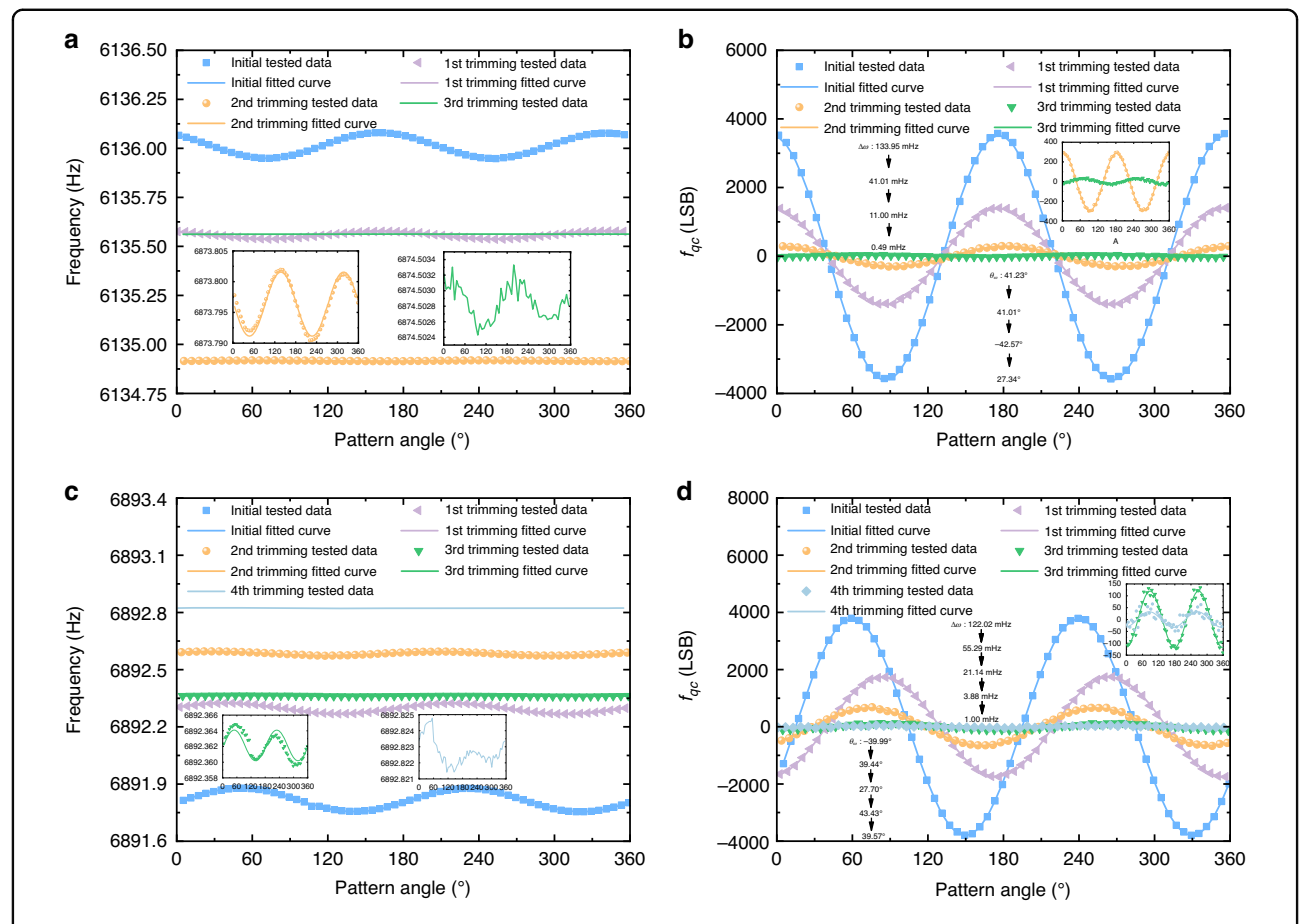


**Fig. 7 The trimming results. a** Test data of frequency during mechanical trimming of MSRG M02. **b** Test data of quadrature-control force  $f_{qc}$  during mechanical trimming of MSRG M03. **c** Test data of frequency during mechanical trimming of MSRG M03. **d** Test data of quadrature-control force  $f_{qc}$  during mechanical trimming of MSRG M03

frequency split characterized based on the quadrature-control force under the self-precession mode is reduced from 129.8~mHz-0.32~mHz, and the azimuth of stiffness axis is kept almost unchanged of near  $-20^\circ$ . For all three trimming processes, the laser parameters were set to a power of 1.5~W, a repetition rate of 33~kHz, and a scanning speed of 120~mm/s, and concentric circles with diameters of 100~um, 60~um, and 30~um were etched respectively. The etched depth and morphology are the combined results of the laser parameters and the etched pattern, which also decided the removing masses. The experimental result shows that the proposed method has excellent performance to achieve frequency mismatch of below 1~mHz of the micro-shell resonator.

In order to to verify the repeatability of the mechanical trimming with high precision below 1 mHz by the new characterization method, the MSRG M02 and M03, with initial frequency splits of 133.95 mHz and 122.02 mHz respectively, are chosen for trimming experiments. The frequency split trimming results of the MSRG M02 is shown in Fig. 7a, b. For the MSRG M02, frequency split is

decreased from 133.95 mHz to  $0.49\,\mathrm{mHz}$  after seven trimming cycles. Similarly, by combining this characterization method with mechanical trimming method, the frequency split of the MSRG M03 is reduced from  $122.02\,\mathrm{mHz} - 1.00\mathrm{mHz}$ , as depicted in Fig. 7c, d. It can be seen that, through the proposed method, applying femtosecond laser etching as a mechanical trimming method to decrease frequency split of micro-shell resonators to achieve below  $1\,\mathrm{mHz}$  grade is not only effective, but also repeatable.

#### Conclusion

This paper presents a 0.32 mHz frequency mismatch of MSRG without tuning electrodes achieved by ultraprecision mechanical trimming. The effect of frequency mismatch on the performance of MSRG is analyzed, and the model of frequency trimming based on mass removal is established to present the characterization precision demand of frequency mismatch. A novel characterization method of frequency mismatch based on the quadrature-control force under the self-precession mode is proposed to

meet the requirement of high-precision mechanical trimming. The complete control system under whole-angle mode is established to analyze the effect of phase errors on characterization accuracy of frequency mismatch, which is then corrected by the phase shift module. Meanwhile, simulations and experiments are also carried out to verify the effectiveness of this novel method. Combining this characterization method with the online femtosecond laser mechanical trimming platform, frequency split trimming below 1 mHz is achieved on three micro-shell resonators. The best result that frequency mismatch of micro-shell resonator is reduced from 129.80 mHz - 0.32 mHz. It is the best performance for mechanical trimming of MSRG so far, which is ten times than the current reported results. In the future, the MSRG without tuning electrodes will hold considerable potential for application in high-precision inertial navigation systems.

## Acknowledgements

This work is supported by the Key Projects of the National Natural Science Foundation of China (51935013, 52205613), and the Regional Innovative Development Joint Funds of the National Natural Science Foundation of China (U21A20505).

#### **Author contributions**

Sheng Yu analyzed the influences of the frequency mismatch in gyroscope performance, proposed the characterization method, and wrote the manuscript, Xianfeng Huang conducted the numerical simulations, theoretical analysis, and experimental tests, Xuezhong Wu and Dingbang Xiao designed the general architecture of the resonator, Peng Xie and Kun Lu fabricated the micro-shell resonator, Jiangkun Sun and Yongmeng Zhang designed the hardware circuits for the realization of the whole-angle MSRG with the implementation of the phase errors correction method. Xianfeng Huang and Sheng Yu contributed equally to this work.

#### Conflict of interest

The authors declare no competing interests.

Received: 15 September 2024 Revised: 15 December 2024 Accepted: 6 January 2025

Published online: 22 May 2025

#### References

- Sun, J. et al. 0.79 ppm scale-factor nonlinearity whole-angle microshell gyroscope realized by real-time calibration of capacitive displacement detection. *Microsyst. Nanoeng.* 7, 129–139 (2021).
- Singh, S. S. et al. 0.0062°/√hr angle random walk and 0.027°/√hr bias instability from a micro-shell resonator gyroscope with surface electrodes. In 2020 33rd IEEE International Conference on Micro Electro Mechanical Systems (MEMS). 737–740 (Vancouver, BC, 2020).
- Meyer, D. & Rozelle, D. Milli-HRG inertial navigation system. Gyro. Nav. 3, 24–29 (2012).
- Chen, Y. et al. Simulated analysis of forming imperfection for micro shell resonators. Microsyst. Technol. 27, 723 (2021).
- Li, B. et al. Frequency split suppression of fused silica micro shell resonator based on rotating forming process. *Microsyst. Technol.* 27, 789–799 (2021).

- Shin, D. D. et al. Electrostatic tuning of temperature coefficient of frequency of anisotropic disk-shaped resonators. In 2017 IEEE International Symposium on Inertial Sensors and Systems (INERTIAL). 164–167 (Kauai, HI, 2017).
- Gallacher, B. J. et al. Electrostatic correction of structural imperfections present in a microring gyroscope. J. Microelectromech. Syst. 14, 221–234 (2005).
- Asadian, et al. Controlled capacitive gaps for electrostatic actuation and tuning of 3D fused quartz micro wineglass resonator gyroscope. In 2017 4th IEEE International Symposium on Inertial Sensors and Systems (INERTIAL). 19–22 (2017).
- Cho, J. Y. et al. 1.5 million Q-factor vacuum-packaged birdbath resonator gyroscope (BRG). In 2019 32nd IEEE International Conference on Micro Electro Mechanical Systems (MEMS). 210–213 (2019).
- Vatanparvar, D. & Shkel, A. M. Instabilities due to electrostatic tuning of frequency-split in coriolis vibratory gyroscopes. In 2020 IEEE SENSORS, 1–4 (2020).
- Lu, K. et al. Research on precise mechanical trimming of a micro shell resonator with T-shape masses using femtosecond laser ablation. Sens. Actuators A: Phys. 290, 228–238 (2019).
- 12. Bernstein, J. J. et al. High Q diamond hemispherical resonators: fabrication and energy loss mechanisms. *J. Micromech. Microeng.* **25**, 1 (2015).
- Hamelin et al. Localized eutectic trimming of polysilicon microhemispherical resonating gyroscopes. IEEE Sens. J. 14, 3498–3505 (2014).
- Lu, K. et al. Achieving sub-5 mHz frequency split trimming of micro hemispherical resonator gyroscope with method of mass-stiffness decoupling. *IEEE Sens. J.* 24, 1 (2024).
- Viswanath, et al. Gianchandani. High resolution micro ultrasonic machining (HR-µUSM) for post-fabrication trimming of fused silica 3-D microstructures. In 2014 27th IEEE International Conference on Micro Electro Mechanical Systems (MEMS). 494–497 (2014).
- Pan, Y. et al. Trimming of imperfect cylindrical fused silica resonators by chemical etching. Sensors 19, 3596 (2019).
- 17. Wang, Y., Asadian, M. H. & Shkel, A. M. In 2017 IEEE International Symposium on Inertial Sensors and Systems (INERTIAL). 78–81 (2017).
- Huo, Y. et al. High precision mass balancing method for the fourth harmonic of mass defect of fused quartz hemispherical resonator based on ion beam etching process. *IEEE Trans. Ind. Electron.* 70, 9601–9613 (2023).
- Zhang, W. et al. The high-precision balance method for hemispherical resonator based on synchronous trimming system. *IEEE Sens. J.* 24, 31780–31788 (2023).
- Zotov, S. A., Trusov, A. A. & Shkel, A. M. Three-dimensional spherical shell resonator gyroscope fabricated using wafer-scale glassblowing. *J. Microelectromech. Syst.* 21, 509–510 (2012).
- Prikhodko, I. P., Zotov, S. A., Trusov, A. A. & Shkel, A. M. Microscale glass-blown three-dimensional spherical shell resonators. *J. Microelectromech. Syst.* 20, 691–701 (2011).
- Lu, K. et al. Micro shell resonator with T-shape masses fabricated by improved process using whirling platform and femtosecond laser ablation. In 2017 IEEE International Symposium on Inertial Sensors and Systems (INERTIAL). 102–104 (2017)
- Asadian, M. H., Wang, Y. & Shkel, A. M. Development of 3D fused quartz hemitoroidal shells for high-Q resonators and gyroscopes. *J. Microelectromech. Syst.* 28, 954–964 (2019).
- Senkal, D. et al. High temperature micro-glassblowing process demonstrated on fused quartz and ULE TSG. Sens. Actuators. A. Phys. 201, 525–531 (2013).
- Shi, Y. et al. Geometric imperfection characterization and precise assembly of micro shell resonators. J. Microelectromech. Syst. 29, 480–489 (2020).
- Hou, Z. et al. A quadrature compensation method to improve the performance of the butterfly vibratory gyroscope. Sens. Acutuators A Phys. 319, 112527 (2021).
- Sun, J. et al. Identification and correction of phase error for whole-angle microshell resonator gyroscope. IEEE Sens. J. 22, 19228–19236 (2022).
- 28. Jeanroy, A., Bouvet, A. & Remillieux, G. HRG and marine applications. *Gyr. Nav.* **5**, 67–74 (2014).
- Fox, C. H. J. A simple theory for the analysis and correction of frequency splitting in slightly imperfect rings. J. Sound Vib. 142, 227–243 (1990).
- Lynch, D. D. Vibratory gyro analysis by the method of averaging. St. Pe-tersburg Conf. Gyr. Technol. Nav. 26, 34 (1995).